

Natural convection heat transfer enhancement in horizontal concentric annuli using nanofluids[☆]

E. Abu-Nada^{*}, Z. Masoud, A. Hijazi

Department of Mechanical Engineering, Hashemite University, Zarqa 13115, Jordan

Available online 6 February 2008

Abstract

Heat transfer enhancement in horizontal annuli using nanofluids is investigated. Water-based nanofluid containing various volume fractions of Cu, Ag, Al₂O₃ and TiO₂ nanoparticles is used. The addition of the different types and different volume fractions of nanoparticles were found to have adverse effects on heat transfer characteristics. For high values of Rayleigh number and high L/D ratio, nanoparticles with high thermal conductivity cause significant enhancement of heat transfer characteristics. On the other hand, for intermediate values of Rayleigh number, nanoparticles with low thermal conductivity cause a reduction in heat transfer. For $Ra=10^3$ and $Ra=10^5$ the addition of Al₂O₃ nanoparticles improves heat transfer. However, for $Ra=10^4$, the addition of nanoparticles has a very minor effect on heat transfer characteristics.
© 2008 Elsevier Ltd. All rights reserved.

Keywords: Nanofluids; Heat transfer enhancement; Natural convection; Concentric annulus

1. Introduction

Heat transfer within horizontal annuli has many engineering applications such as heat exchangers, solar collectors, thermal storage systems, and cooling of electronic components. Several applications use natural convection as the main heat transfer mechanism. Therefore, it is important to understand the thermal behavior of such systems when only natural convection is in effect so that methods to enhance heat transfer characteristics in such systems can be devised.

The geometric shape of the cylindrical annulus creates non-uniformity in heat transfer within the annulus. With a better understanding of the flow field, it is possible to devise methods for heat transfer enhancement. An innovative technique for improving heat transfer is using ultra fine solid particles in the base fluids, which has been used extensively in the past ten years. The term nanofluid refers to fluids in which nano-scale particles are suspended in the base fluid [1]. The particles are

different from conventional particles (millimeter or micro-scale) in that they tend to remain suspended in the fluid and no sedimentation occur which causes no increase in pressure drop in the flow field [2].

The past decade has witnessed extensive work on convective heat transfer using nanofluids. Studies on the enhancement of heat transfer characteristics in forced convection applications were conducted by a number of researchers. On the other hand, heat transfer enhancement in natural convection applications has received little attention. Examples of the work conducted on natural convection heat transfer include the work of Khanafer et al. [3] who studied Copper–Water nanofluids in a two dimensional rectangular enclosure. They found that the heat transfer rate increased by increasing the percentage of the suspended particles. Similar enhancement was achieved experimentally by Nnanna et al. [4] for Cu nanoparticles in ethylene glycol and by Nnanna and Routhu [5] for Alumina–Water nanofluids. However, different experimental findings were reported by Putra et al. [6] on the natural convection of Al₂O₃– and CuO–Water nanofluids inside a cylindrical enclosure heated from one side and cooled from the other. They found that the natural convection heat transfer coefficient was lower than that of pure water. Wen and Ding [7] found that the natural convection heat transfer coefficient

[☆] Communicated by W.J. Minkowycz.

^{*} Corresponding author.

E-mail address: eyiad@hu.edu.jo (E. Abu-Nada).

Nomenclature

b	source term
c_p	specific heat at constant pressure
D	diameter of inner cylinder
g	gravitational acceleration
h	local heat transfer coefficient
k	thermal conductivity
L	gap between inner and outer cylinder, i.e., $L=r_o-r_i$
Nu	Nusselt number
n	particle shape factor
Pr	Prandtl number,
q_w	heat transfer at the cylinder wall
Ra	Rayleigh number,
\tilde{r}	radial coordinate measured from the inner cylinder surface
r	nondimensional radial distance,
\tilde{T}	dimensional temperature
T	nondimensional temperature,
u	dimensional tangential velocity
U	nondimensional tangential velocity,
v	dimensional radial velocity
V	nondimensional radial velocity,

Greek symbols

α	thermal diffusivity
β	thermal expansion coefficient
ε	numerical tolerance
η	coordinates in computational plane
φ	nanoparticle volume fraction
ϕ	transport quantity
ν	kinematic viscosity
θ	angle measured from the lower plane
Ψ	nondimensional stream function,
ψ	dimensional stream function
Ω	nondimensional vorticity,
ω	dimensional vorticity
ρ	density
μ	dynamic viscosity
ξ	coordinate in computational plane

Subscripts

f	fluid
i	inner
nf	nanofluid
o	outer
s	solid

Recently, Trisaksri and Wongwises [9], and Wang and Mujumdar [10] conducted a literature review on the general heat transfer characteristics of nanofluids. Daungthongsuk and Wongwises [2] performed a comprehensive review of convective heat transfer of nanofluids. Based on literature reviews, no work has focused on natural convection heat transfer enhancement within a concentric cylindrical annulus. Therefore, the goal of this work is to investigate heat transfer characteristics of natural convection in the annulus between horizontal concentric cylinders using different types of nanofluids. The problem will be investigated numerically by solving the Navier–Stokes and energy equations (NSE) using the finite volume technique. Heat transfer characteristics will be analyzed using a wide range of volume fractions of nanoparticles at various Rayleigh numbers.

2. Problem description and governing equations

Due to geometrical symmetry, Fig. 1, only one half of the annulus is simulated. The annulus between the two cylinders is filled with water based nanofluid. Four types of nanoparticles (Al_2O_3 , Cu, Ag, and TiO_2) are investigated. It was assumed that the flow is steady, and that the base fluid and the nanoparticles are in thermal equilibrium and no slip occurs between them. Thermo-physical properties of the nanofluid are assumed to be constant except for the density variation, which is approximated by the Boussinesq model. The thermo-physical properties of the base fluid and the different types of nanoparticles as well as air which were used for code validation are given in Table 1. The inner cylinder surface is maintained at a constant temperature T_i which is higher than the outer cylinder temperature T_o . The governing equations for the laminar natural convection in terms of stream function-vorticity formulation are the vorticity equation, the energy equation, and the kinematics equation respectively:

$$\begin{aligned} & \frac{\partial}{\partial \tilde{r}} \left(\omega \frac{\partial \Psi}{\partial \theta} \right) - \frac{\partial}{\partial \theta} \left(\omega \frac{\partial \Psi}{\partial \tilde{r}} \right) \\ &= \frac{\mu_{\text{nf}}}{\rho_{\text{nf}}} \left(\frac{\partial}{\partial \tilde{r}} \left(\tilde{r} \frac{\partial \omega}{\partial \tilde{r}} \right) + \frac{\partial}{\partial \theta} \left(\frac{1}{\tilde{r}} \frac{\partial \omega}{\partial \theta} \right) \right) \\ &+ \frac{(\varphi \rho_s \beta_s + (1 - \varphi) \rho_f \beta_f)}{\rho_{\text{nf}}} g \left(\frac{\partial \tilde{T}}{\partial \tilde{r}} \tilde{r} \sin \theta + \frac{\partial \tilde{T}}{\partial \theta} \cos \theta \right) = 0 \end{aligned} \quad (1)$$

$$\begin{aligned} \frac{\partial}{\partial \tilde{r}} \left(\tilde{T} \frac{\partial \Psi}{\partial \theta} \right) - \frac{\partial}{\partial \theta} \left(\tilde{T} \frac{\partial \Psi}{\partial \tilde{r}} \right) &= \frac{\partial}{\partial \tilde{r}} \left(\alpha_{\text{nf}} \tilde{r} \frac{\partial \tilde{T}}{\partial \tilde{r}} \right) \\ &+ \frac{\partial}{\partial \theta} \left(\alpha_{\text{nf}} \frac{1}{\tilde{r}} \frac{\partial \tilde{T}}{\partial \theta} \right) \end{aligned} \quad (2)$$

$$\frac{\partial}{\partial \tilde{r}} \left(\tilde{r} \frac{\partial \Psi}{\partial \tilde{r}} \right) + \frac{\partial}{\partial \theta} \left(\frac{1}{\tilde{r}} \frac{\partial \Psi}{\partial \theta} \right) = -\tilde{r} \omega \quad (3)$$

$$\text{where } \alpha_{\text{nf}} = \frac{k_{\text{nf}}}{(\rho c_p)_{\text{nf}}}.$$

in a vessel composed of two discs using TiO_2 nanoparticles decreases by increasing the volume fraction of nanoparticles. Jou and Tzeng [8] simulated natural convection heat transfer of Copper–Water nanofluids in a two dimensional enclosure. They reported an increase in heat transfer by the addition of nanoparticles.

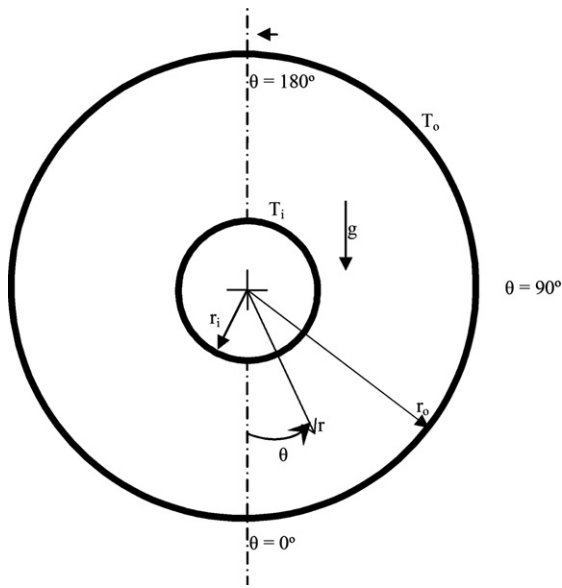


Fig. 1. Sketch of problem geometry.

The viscosity of the nanofluid is approximated by the viscosity of a base fluid μ_f containing diluted suspension of fine spherical particles and is given by [11]:

$$\mu_{nf} = \frac{\mu_f}{(1 - \phi)^{2.5}} \tag{4}$$

The density of the nanofluid is given by:

$$\rho_{nf} = (1 - \phi)\rho_f + \phi\rho_s \tag{5}$$

The heat capacitance of the nanofluid is expressed as:

$$(\rho c_p)_{nf} = (1 - \phi)(\rho c_p)_f + \phi(\rho c_p)_s \tag{6}$$

The effective thermal conductivity of the nanofluid is approximated by the Hamilton–Crosser model [12] as:

$$\frac{k_{nf}}{k_f} = \frac{k_s + (n - 1)k_f - (n - 1)(k_f - k_s)\phi}{k_s + (n - 1)k_f + (k_f - k_s)\phi} \tag{7}$$

where n is the nanoparticle shape factor which is set equal to 3 for spherical nanoparticles. The use of this equation is restricted to spherical nanoparticles where it does not account for other shapes of nanoparticles. This model is found to be appropriate

for studying heat transfer enhancement using nanofluids [13–16].

The radial and tangential velocities are given by the following relations, respectively:

$$v = \frac{1}{\tilde{r}} \frac{\partial \psi}{\partial \theta} \text{ and } u = -\frac{\partial \psi}{\partial \tilde{r}} \tag{8}$$

The following dimensionless group is introduced

$$\Omega = \frac{\omega L^2}{\alpha_f}, \Psi = \frac{\psi}{\alpha_f}, V = \frac{vL}{\alpha_f}, U = \frac{uL}{\alpha_f}, T = \frac{\tilde{T} - T_o}{T_i - T_o}, \text{ and } r = \frac{\tilde{r} - r_i}{L}$$

Also, the following transformation is used:

$$r = \frac{(2\alpha - \beta) + (2\alpha + \beta) \left(\frac{\beta + 1}{\beta - 1} \right)^{\left(\frac{\xi - \sigma}{1 - \sigma} \right)}}{(2\alpha + 1) \left(1 + \left(\frac{\beta + 1}{\beta - 1} \right)^{\left(\frac{\xi - \sigma}{1 - \sigma} \right)} \right)} \tag{9}$$

$$\theta = \pi\eta$$

This transformation ensures a fine grid (a stretched grid) close to the inner and to the outer cylinders surfaces, which can resolve the steep velocity and temperature gradients at these surfaces. This grid stretching method results in considerable savings in terms of the grid size and the computational time [17]. By using the mentioned transformation the physical domain (r, θ) is transformed into a uniform grid in the computational (ξ, η) domain (see Fig. 2).

By using the dimensionless parameters and the transformation given in Eq. (9), the governing equations are rewritten as:

$$\frac{1}{Pr\pi} \left[\frac{\partial}{\partial \xi} \left(\Omega \frac{\partial \Psi}{\partial \eta} \right) - \frac{\partial}{\partial \eta} \left(\Omega \frac{\partial \Psi}{\partial \xi} \right) \right] = \tau G(\Omega) + \delta Ra \left[\frac{\partial r}{\partial \xi} \cos(\pi\eta) \frac{\partial T}{\partial \eta} + \left(r + \frac{r_i}{L} \right) \sin(\pi\eta) \frac{\partial T}{\partial \xi} \right] \tag{10}$$

$$\frac{1}{\lambda\pi} \left[\frac{\partial}{\partial \xi} \left(T \frac{\partial \Psi}{\partial \eta} \right) - \frac{\partial}{\partial \eta} \left(T \frac{\partial \Psi}{\partial \xi} \right) \right] = G(T) \tag{11}$$

$$\Omega = \frac{-1}{\frac{\partial r}{\partial \xi} \left(r + \frac{r_i}{L} \right)} G(\psi) \tag{12}$$

Table 1
Thermo-physical properties

		Pr	ρ (kg/m ³)	c_p (J/kg K)	k (W/m K)	$\beta \times 10^{-5}$ (K ⁻¹)	$\alpha \times 10^{-5}$ (m ² /s)
Base fluids	Air	0.7	1.2	1006	0.026	340	
	Water	6.2	997.1	4179	0.613	21	
Nano-particles	Copper (Cu)		8933	385	401	1.67	11.7
	Silver (Ag)		10500	235	429	1.89	17.4
	Alumina (Al ₂ O ₃)		3970	765	40	0.85	1.3
	Titanium Oxide (TiO ₂)		4250	686.2	8.9538	0.9	0.31

where

$$G(Q) = \frac{1}{\frac{\partial r}{\partial \xi}} \left(r + \frac{r_i}{L} \right) \frac{\partial^2 Q}{\partial \xi^2} + \left(1 + r \frac{\partial^2 \xi}{\partial r^2} \frac{\partial r}{\partial \xi} + r \frac{\partial}{\partial \xi} \left(\frac{\partial \xi}{\partial r} \right) \right. \\ \left. + \frac{\partial r}{\partial \xi} \left(\frac{\partial^2 \xi}{\partial r^2} + \frac{\partial r}{\partial \xi} \frac{\partial}{\partial \xi} \left(\frac{\partial \xi}{\partial r} \right) \right) \left(\frac{r_i}{L} \right) \right) \frac{\partial Q}{\partial \xi} - \frac{\frac{\partial r}{\partial \xi}}{\pi^2 \left(r + \frac{r_i}{L} \right)} \frac{\partial^2 Q}{\partial \eta^2}$$

$$\tau = \frac{1}{(1-\varphi)^{0.25} \left((1-\varphi) + \varphi \frac{\rho_s}{\rho_f} \right)}, \delta = \frac{1}{\frac{(1-\varphi)\rho_r}{\varphi\rho_s} + 1} \beta_s + \frac{1}{\frac{\varphi}{(1-\varphi)} \frac{\rho_s}{\rho_f} + 1},$$

$$\text{Pr} = \frac{\nu_f}{\alpha_f}, \text{Ra} = \frac{g\beta(T_w - T_\infty)L^3}{\nu_f \alpha_f}, \text{ and } \lambda = \frac{\frac{k_{nf}}{k_f}}{(1-\varphi) + \varphi \frac{(\rho c_p)_s}{(\rho c_p)_f}}.$$

The velocities are written in a non-dimensional form in the computational domain as:

$$V = \frac{1}{\pi \left(r + \frac{r_i}{L} \right)} \frac{\partial \Psi}{\partial \eta} \tag{13}$$

$$U = -\frac{1}{\frac{\partial r}{\partial \xi}} \frac{\partial \Psi}{\partial \xi} \tag{14}$$

The dimensionless boundary conditions are as follows:

$$\left. \begin{aligned} &\text{On the inner cylinder surface, } \Psi = 0, \\ &\omega = -\frac{1}{\left(\frac{\partial r}{\partial \xi} \right)^2} \frac{\partial^2 \Psi}{\partial \xi^2}, \text{ and } T = 1. \\ &\text{On the outer cylinder surface, } \Psi = 0, \\ &\omega = -\frac{1}{\left(\frac{\partial r}{\partial \xi} \right)^2} \frac{\partial^2 \Psi}{\partial \xi^2}, \text{ and } T = 0. \\ &\text{Symmetry lines : } \Psi = 0, \Omega = 0, \text{ and } \frac{\partial T}{\partial \eta} = 0. \end{aligned} \right\} \tag{15}$$

3. Numerical implementation

Eqs. (10) through (12), with the corresponding boundary conditions given in Eq. (15), are solved using the finite volume approach [18,19]. The diffusion term in the vorticity, energy, and kinematic equations is approximated by a second-order central difference which gives a stable solution. Furthermore, a second order upwind differencing scheme is adopted for the convective terms. The resulting algebraic equations are solved using successive over/under relaxation method. Successive under relaxation was used due to the non-linear nature of the governing equations especially for the vorticity equation. A fourth order accurate formula for the vorticity boundary condition at the wall is adopted [20]:

$$\Omega_{0,j} = -\frac{(108\Psi_{1,j} - 27\Psi_{2,j} + 4\Psi_{3,j})}{18(\Delta\xi)^2 \left(\frac{\partial r}{\partial \xi} \right)^2}. \tag{16}$$

After solving for Ψ , Ω , and T , further useful quantities are obtained. For example, Nusselt number can be expressed as:

$$\text{Nu} = -\frac{2}{\frac{\partial r}{\partial \xi}} \left(\frac{r_i}{L} \right) \left(\frac{k_{nf}}{k_f} \right) \frac{\partial T}{\partial \xi}. \tag{17}$$

The average Nusselt number on the inner cylinder surface is evaluated as:

$$\text{Nu}_{\text{avg}} = \int_{\eta=0}^{\eta=1} \text{Nu}(\eta) d\eta. \tag{18}$$

1/3rd Simpson’s rule of integration is used to evaluate Eq. (18). The Nusselt number is used as an indicator of heat transfer enhancement where an increase in Nusselt number corresponds to enhancement in heat transfer.

4. Grid testing and code validation

An extensive mesh testing procedure was conducted to guarantee a grid independent solution. Two cases of $\text{Ra} = 0.53 \times 10^4$ and $\text{Ra} = 10^5$ using $\text{Pr} = 0.7$ are tested for grid independence with no nanoparticles in the flow field. The present code was tested for grid independence by calculating the average Nusselt number around the inner cylinder surface. It was found that a grid size of 61×61 guarantees a grid independent solution for both cases. The Nusselt number for the grid independent solution is compared with the results of Guj and Stella [21] and Shu et al. [22] for concentric horizontal annulus and $\text{Ra} = 0.53 \times 10^4$. The calculated average Nusselt number by the current code gives a value of 2.47010 which falls between the results obtained by Guj and Stella ($\text{Nu}_{\text{avg}} = 2.4220$) and the results of Shu et al. ($\text{Nu}_{\text{avg}} = 2.5560$). Furthermore, a grid independence test was carried out for the nanofluid case for water as the base fluid, Al_2O_3 nanoparticles, $\varphi = 0.10$, $\text{Ra} = 10^5$, and $L/D = 0.8$. It was found that a grid size of 61×61 guarantees a grid independent solution.

Due the lack of experimental data for natural convection in an annulus with the presence of nanoparticles, the present numerical solution is validated by the experimental results of Kuhen and Goldstein [23] using $\text{Ra} = 4.57 \times 10^4$ and $\text{Pr} = 0.7$. Three temperature profiles at three different angles are shown in [25]. The present results are in good agreement with other published data.

5. Results and discussion

The range of Rayleigh number, volume fraction of nanoparticles, and L/D ratio are $\text{Ra} = 10^3 - 10^5$, $0 \leq \varphi \leq 0.1$, and $0.2 \leq L/D \leq 0.8$, respectively. The Prandtl number of the base fluid is kept constant at 6.2. Fig. 3 presents Nusselt number distribution around the inner cylinder surface using various volume fractions of Al_2O_3 nanoparticles. Fig. 3(a) shows the variation using $L/D = 0.8$ and $\text{Ra} = 10^5$. The figure shows that, around the inner cylinder surface, there are locations where the Nusselt number distribution is affected by the presence of

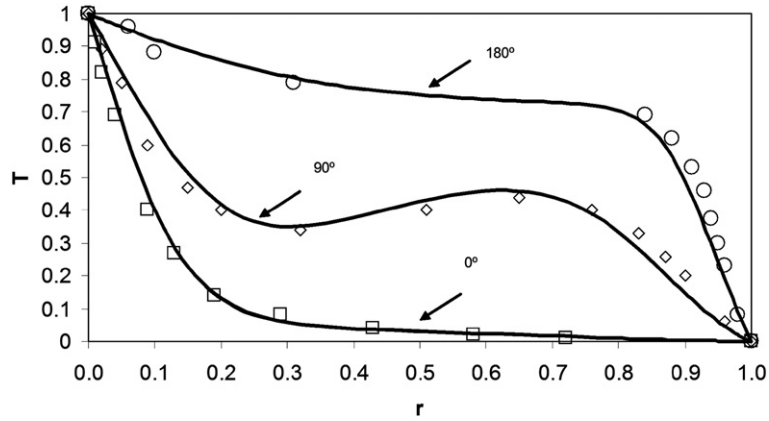


Fig. 2. Comparison of the results of the present work (solid lines) and Kuhen and Goldstein [24] experimental results, experimental data points: \square : 0° , \diamond : 90° , \circ : 180° ($Ra=4.7 \times 10^4$, $Pr=0.706$, and $L/D=0.8$).

nanoparticles and other locations (such as the plume region) where Nusselt number is not affected. The intensity of the plume increases with the addition of nanoparticles as shown in Fig. 4(a) and (b). The dependency of Nusselt number on the nanoparticle volume fraction can be further explained by examining Eq. (17). The equation shows that the Nusselt number is influenced by two parameters, which are the

temperature gradient at the cylinder surface and the thermal conductivity ratio (note that other parameters are constants). Fig. 5 quantifies the weight of these two parameters. It is clear from Fig. 5(a) that as the percentage of the Al_2O_3 nanoparticles increases, the temperature gradient decreases. This decrease is due to the enhanced effective thermal conductivity of the nanofluid which is accompanied by an increase in the thermal

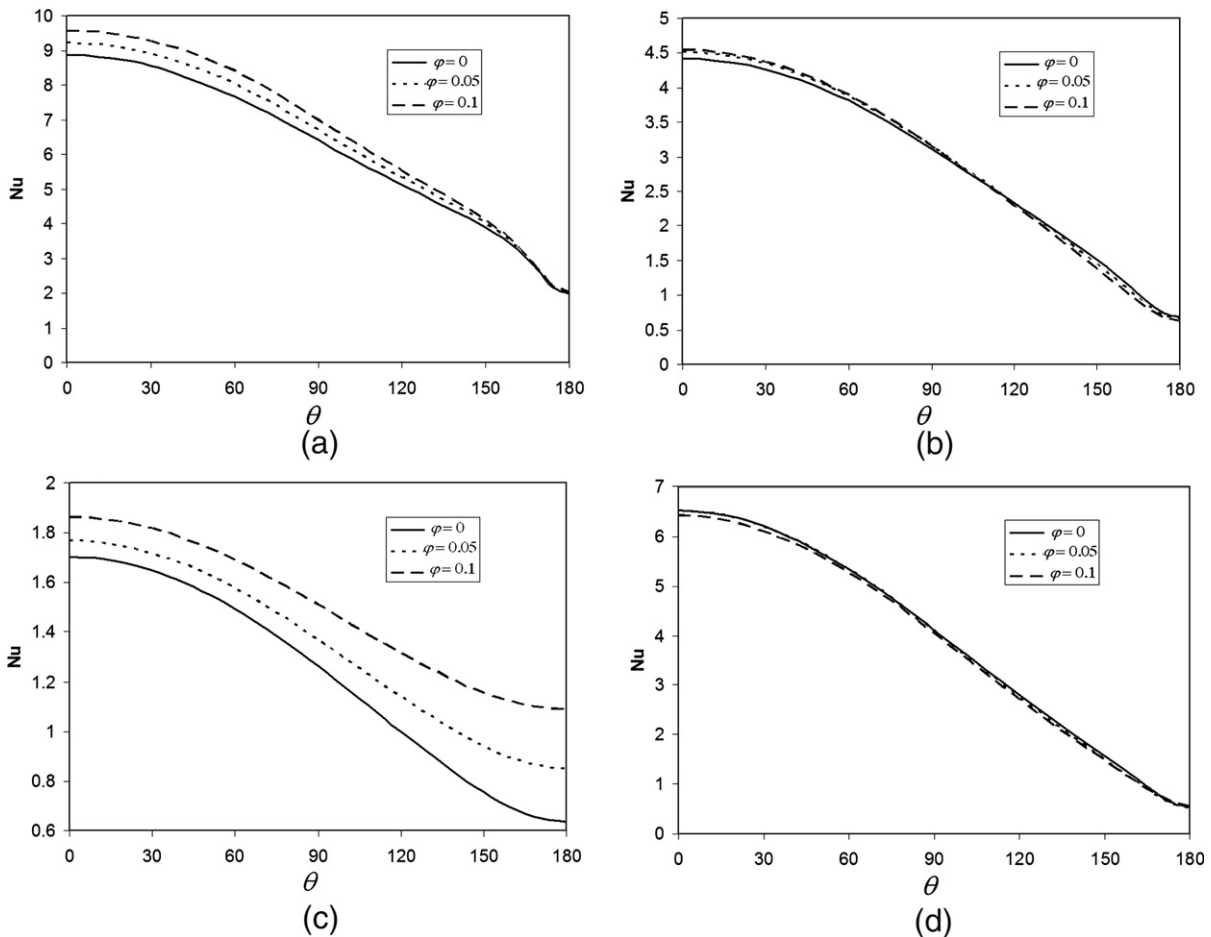


Fig. 3. Nusselt number distribution around inner cylinder surface using various volume fractions of Al_2O_3 nanoparticles (a) $Ra=10^5$, $L/D=0.8$ (b) $Ra=10^4$, $L/D=0.8$ (c) $Ra=10^3$, $L/D=0.8$ (d) $Ra=10^4$, $L/D=0.4$.

diffusivity (see Fig. 5(b) and (c)). The increase in thermal diffusivity causes the drop in the temperature gradients. By inspecting Fig. 5(a) and (b) it is clear that outside the plume region, the increase in thermal conductivity ratio is greater than the decrease in temperature gradient. For example, at $\theta=0$ and when the volume fraction of the nanoparticles is increased from zero to 10%, the temperature gradient is decreased by approximately 20% and the thermal conductivity ratio of the nanofluid is increased by about 30%. Accordingly, the Nusselt number increases by increasing the volume fraction of the nanoparticles. However, within the plume region, the reduction in temperature gradient becomes approximately equal to the enhancement in the effective thermal conductivity which explains the independency of the Nusselt number from the volume fraction of the nanoparticles in the plume region.

Fig. 3(b) shows that the region that experience enhancement in heat transfer becomes narrower. For this Rayleigh number, the plume region and the thermal boundary layer become wider. For example, for $\theta > 110^\circ$, the nanoparticles cause a decrease in Nusselt number. Fig. 3(c) shows that the presence of

nanoparticles for $Ra=10^3$ always increase Nusselt number and this increase become more pronounced in the plume region. The behavior in the plume region for $Ra=10^3$ is different from that of $Ra=10^5$. The inertia forces at $Ra=10^3$, are small and the conduction heat transfer become more significant due to the addition of nanoparticles. This will reduce the size of the plume and the size of the boundary layer which will increase the value of Nusselt number, Fig. 4(c) and (d). Fig. 3(d) shows that the addition of nanoparticles has an adverse effect on Nusselt number for $Ra=10^4$ and $L/D=0.4$.

An interesting comparison between various nanofluids is presented in Fig. 6. The figure shows that nanoparticles with high thermal conductivity cause significant enhancement in heat transfer characteristics. However, within the plume region the effect of the nanoparticles type is less pronounced. The figure also shows the case of $Ra=10^3$ and $L/D=0.8$ where nanoparticles with high thermal conductivity cause more enhancement of heat transfer characteristics. However, an interesting observation which is worth mentioning is that although Al_2O_3 has a low thermal conductivity, it shows higher

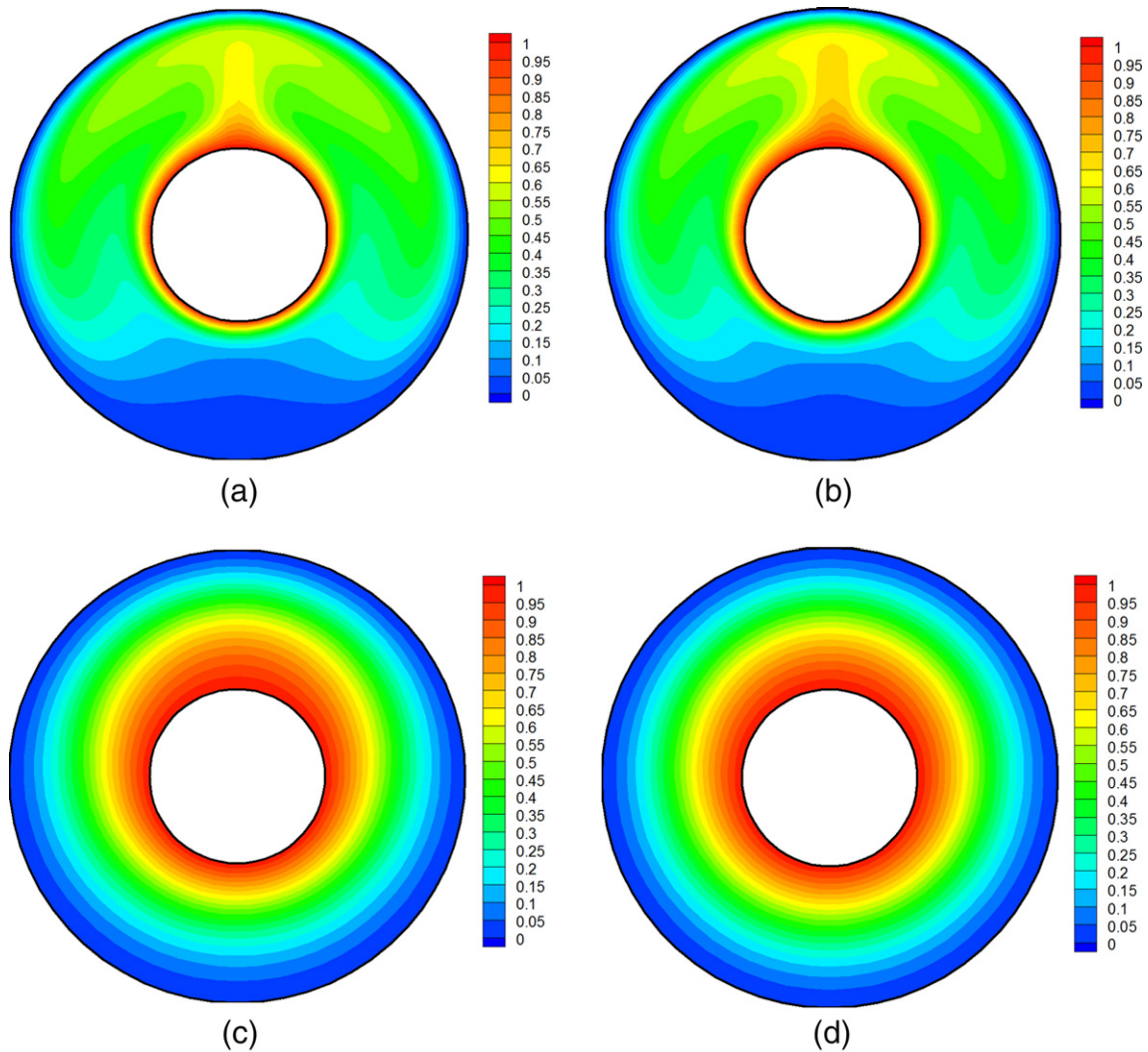


Fig. 4. Temperature isotherms using Al_2O_3 nanoparticles (a) $Ra=10^5$, $L/D=0.8$, $\phi=0$ (b) $Ra=10^5$, $L/D=0.8$, $\phi=0.10$ (c) $Ra=10^3$, $L/D=0.8$, $\phi=0$ (d) $Ra=10^3$, $L/D=0.8$, $\phi=0.10$.

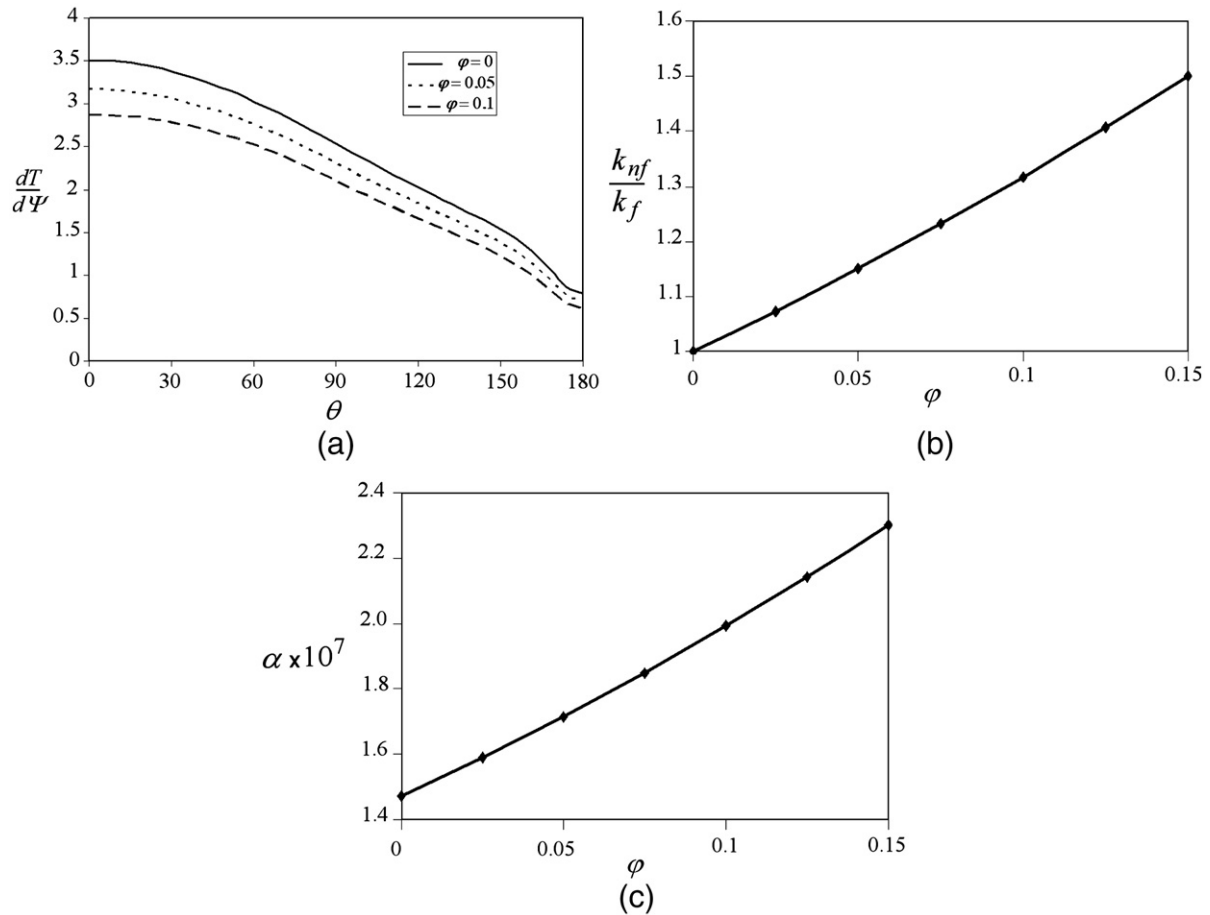


Fig. 5. (a) Temperature gradient at the cylinder surface using Al_2O_3 nanoparticles, $\text{Ra}=10^5$, $L/D=0.8$, $\varphi=0.10$ (b) Effect of volume fraction of Al_2O_3 nanoparticles on thermal conductivity ratio (b) Effect of volume fraction of Al_2O_3 nanoparticles on thermal diffusivity.

enhancement of heat transfer characteristics in the plume region compared to the high thermal conductivity metals, such as Cu or Ag. The thermal conductivity of Al_2O_3 is approximately one tenth of Cu, as given in Table 1. However, a unique property of Al_2O_3 is its low thermal diffusivity, Table 1. The reduced value of thermal diffusivity leads to higher temperature gradients and therefore, more enhancement in heat transfer. Cu and Ag have high values of thermal diffusivity and, therefore, this reduces temperature gradients which will affect the performance of Cu and Ag nanoparticles in the plume region. Fig. 6(c) shows the case of $\text{Ra}=10^4$ and $L/D=0.4$. In this case, nanoparticles such as TiO_2 and Al_2O_3 reduce the Nusselt number and nanoparticles such as Cu and Ag increase the Nusselt number. For TiO_2 and Al_2O_3 nanoparticles, the decrease in temperature gradients is greater than the increase in thermal conductivity ratio. Actually, the increase in thermal conductivity ratio due to the presence of TiO_2 and Al_2O_3 is not large because of the relatively low value of thermal conductivity of those nanoparticles. On the contrary, Cu and Ag nanoparticles have high values of thermal conductivity which will increase the Nusselt number compared to pure water case. However, the difference in heat transfer enhancement by using different types of nanoparticles is small.

Fig. 7 shows the variation of average Nusselt number with different volume fractions of Al_2O_3 nanoparticles for $L/D=0.8$.

It shows that for $\text{Ra}=10^5$ and $\text{Ra}=10^3$, the addition of nanoparticles increases the average Nusselt number. However, for $\text{Ra}=10^4$, a minor effect on the average Nusselt number is observed. Also, it is worth mentioning that for $\text{Ra}=10^4$ and $L/D=0.4$, the addition of nanoparticles reduces the average Nusselt number where the average Nusselt number at $\varphi=0.1$ is equal to 3.855 and the Nusselt number at $\varphi=0$ is 3.940. For this combination of Rayleigh number and L/D ratio, the thermal boundary layer becomes thicker (see Fig. 7(b) and (c)). Therefore, temperature gradients become smaller and the increase in thermal conductivity ratio is still small due to the low thermal conductivity of Al_2O_3 nanoparticles. Accordingly, the presence of nanoparticles decrease the Nusselt number.

6. Conclusions

The main conclusions are summarized as follows:

- For high values of Rayleigh number and L/D ratio, an enhancement in heat transfer is achieved around the inner cylinder surface due to the presence of Al_2O_3 nanoparticles except in the plume region.
- For intermediate values of Rayleigh number ($\text{Ra}=10^4$) the effect of Al_2O_3 nanoparticles on Nusselt number is less

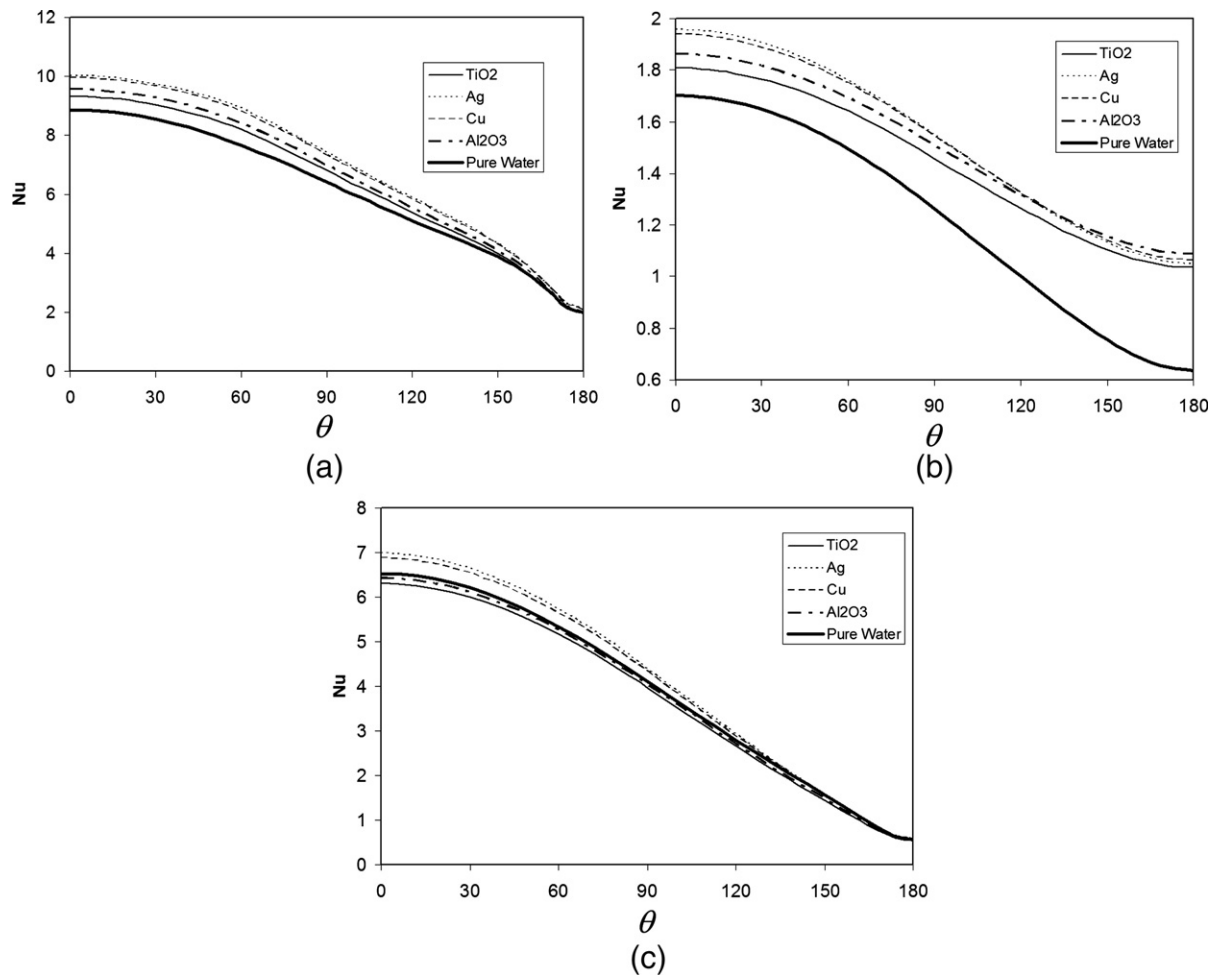


Fig. 6. Nusselt number distribution using different types of nanoparticles $\phi=0.10$ (a) $Ra=10^5, L/D=0.8$ (b) $Ra=10^3, L/D=0.8$ (c) $Ra=10^4, L/D=0.4$.

pronounced, and even a reduction in the Nusselt number is observed for $L/D=0.4$.

- For low Rayleigh number, the addition of Al₂O₃ nanoparticles causes an increase in Nusselt number all over the region around the inner cylinder surface.
- For high Rayleigh number and high L/D ratio, nanoparticles with high thermal conductivity result in significant enhancement in heat transfer.
- For intermediate value of Rayleigh number, nanoparticles with low thermal conductivity show adverse effect on the Nusselt number, especially for $L/D=0.4$.
- For low Rayleigh number, nanoparticles with high thermal conductivity cause more enhancement in heat transfer. However, Al₂O₃ causes more enhancement in heat transfer in the plume region.

References

- [1] S. Lee, S.U.S. Choi, J.A. Eastman, Measuring thermal conductivity of fluids containing oxide nanoparticles, *Journal of Heat Transfer* 121 (1999) 280–289.
- [2] W. Daungthongsuk, S. Wongwises, A critical review of convective heat transfer nanofluids, *Renewable and Sustainable Energy Reviews* 11 (2007) 797–817.
- [3] K. Khanafer, K. Vafai, M. Lightstone, Buoyancy-driven heat transfer enhancement in a two-dimensional enclosure utilizing nanofluids, *International Journal of Heat and Mass Transfer* 46 (2003) 3639–3653.
- [4] A.G.A. Nanna, T. Fistrovich, K. Malinski, S.U.S. Choi, Thermal transport phenomena in buoyancy-driven nanofluids, *Proc. ASME Int. Mech. Eng. Congress RD&D Expo., IMECE2004-62059*, Anaheim, CA, 2004, pp. 1–8.
- [5] A.G.A. Nnanna, M. Routhu, Transport phenomena in buoyancy driven nanofluids – Part II, *Proc. ASME Summer Heat Transfer Conf., SHTC—72782*, San Francisco, CA, 2005, pp. 1–8.
- [6] N. Putra, W. Roetzel, S.K. Das, Natural convection of nanofluids, *Heat and Mass Transfer* 39 (8–9) (2003) 775–784.
- [7] D. Wen, Y. Deng, Formulation of nanofluids for natural convective heat transfer applications, *International Journal of Heat and Fluid Flow* 26 (6) (2005) 855–864.
- [8] R.-Y. Jou, S.-C. Tzeng, Numerical research of nature convective heat transfer enhancement filled with nanofluids in a rectangular enclosure, *International Communications in Heat and Mass Transfer* 33 (2006) 727–736.
- [9] V. Trisaksri, S. Wongwises, Critical review of heat transfer characteristics of nanofluids, *Renewable and Sustainable Energy Reviews* 11 (2007) 512–523.
- [10] X.-Q. Wang, A.S. Mujumdar, Heat transfer characteristics of nanofluids: a review, *International Journal of Thermal Sciences* 46 (2007) 1–19.
- [11] H.C. Brinkman, The viscosity of concentrated suspensions and solutions, *Journal of Chemical Physics* 20 (1952) 571–581.
- [12] R.L. Hamilton, O.K. Crosser, Thermal conductivity of heterogeneous two-component system, *I&EC Fundamentals* 1 (1962) 187–191.

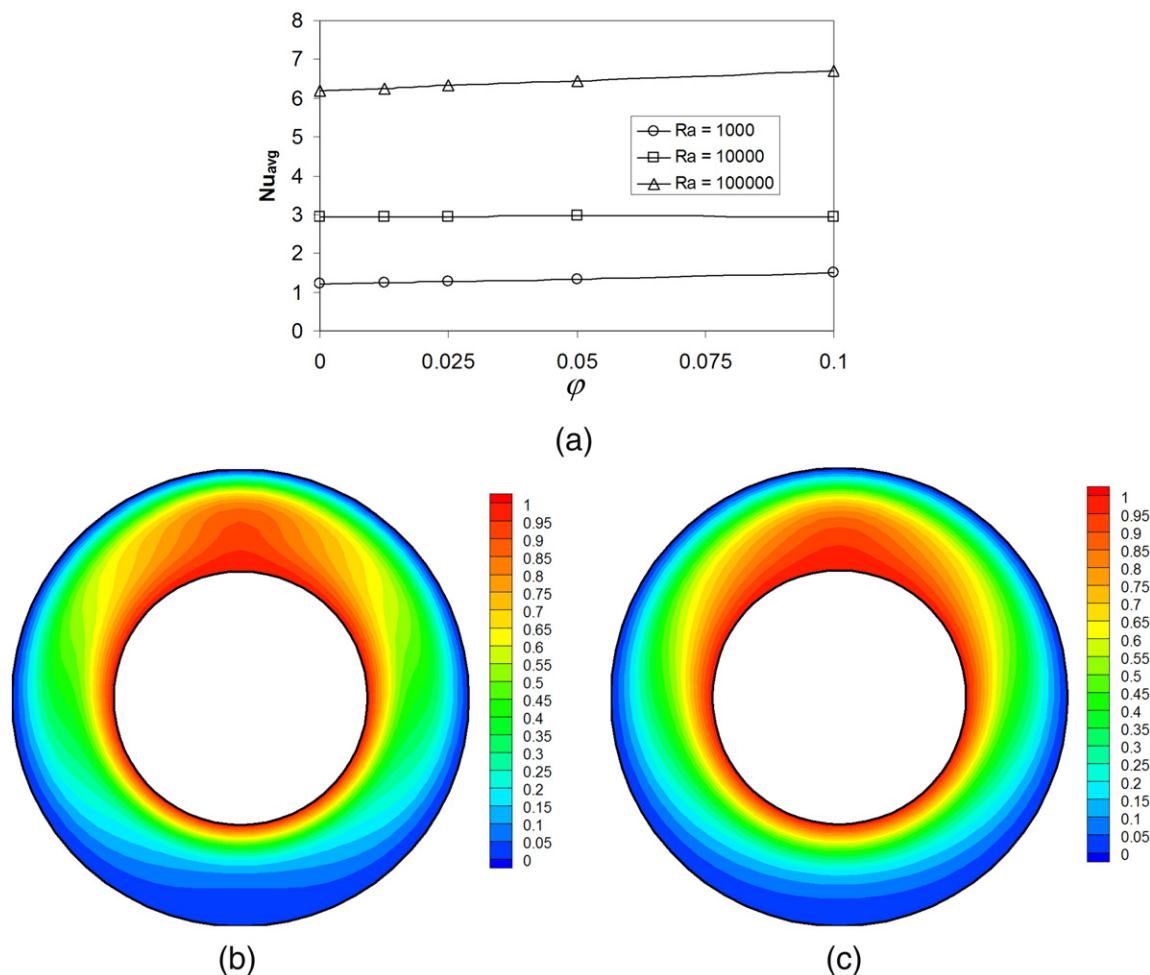


Fig. 7. (a) Average Nusselt number versus volume fraction of Al_2O_3 nanoparticles, $L/D=0.8$ and $\phi=0.10$, (b) Temperature isotherms $Ra=10^4$, $L/D=0.4$ $\phi=0$ (c) temperature isotherms $Ra=10^4$, $L/D=0.4$, $\phi=0.10$.

- [13] Y. Xuan, W. Roetzel, Conceptions for heat transfer correlations of nanofluids, *International Journal of Heat and Mass Transfer* 43 (2000) 3701–3707.
- [14] S.E.B. Maiga, C.T. Nguyen, N. Galanis, G. Roy, Heat transfer behaviors of nanofluids in a uniformly heated tube, *Superlattices and Microstructures* 35 (2004) 543–557.
- [15] G. Roy, C.T. Nguyen, P.R. Lajoie, Numerical investigation of laminar flow and heat transfer in a radial flow cooling system with the use of nanofluids, *Superlattices and Microstructures* 35 (2004) 497–511.
- [16] A. Akbarinia, A. Behzadmehr, Numerical study of laminar mixed convection of a nanofluid in horizontal curved tubes, *Applied Thermal Engineering* 27 (2007) 1327–1337.
- [17] J.D. Anderson, *Computational Fluid Dynamic: The Basics with Applications*, McGraw-Hill, New York, 1995.
- [18] S.V. Patankar, *Numerical Heat Transfer and Fluid Flow*, Hemisphere Publishing Corporation, Taylor and Francis Group, New York, 1980.
- [19] H.K. Versteeg, W. Malalasekera, *An Introduction to Computational Fluid Dynamic: The Finite Volume Method*, John Wiley & Sons Inc, New York, 1995.
- [20] E. Weinan, Jian-Guo Liu, Vorticity boundary condition and related issues for finite difference schemes, *Journal of Computational Physics* 124 (1996) 368–382.
- [21] G. Guj, F. Stella, Natural convection in horizontal eccentric annuli: numerical study, *Numerical Heat Transfer* 27 (1995) 89–105.
- [22] C. Shu, K.S. Yeo, Q. Yao, An efficient approach to simulate natural convection in arbitrary eccentric annuli by vorticity stream function formulation, *Numerical Heat Transfer* 38 (A) (2000) 739–756.
- [23] T.H. Kuhen, R.J. Goldstein, An experimental and theoretical study of natural convection in the annulus between horizontal concentric cylinders, *Journal of Fluid Mechanics* 74 (1976) 695–719.
- [24] T.H. Kuhen, R.J. Goldstein, Numerical solutions to the Navier–Stokes equations for laminar natural convection, *International Journal of Heat and Mass Transfer* 23 (1980) 971–979.
- [25] P. Wang, R. Kahawita, T.H. Nguyen, Numerical computation of the natural convection flow about a horizontal cylinder using splines, *Numerical Heat Transfer* 17 (A) (1990) 191–215.